Effect of Al substitution on the magnetocaloric properties of Ni-Co-Mn-Sn multifunctional alloys

L. Huang[1,2], D. Y. Cong[2,*], Y. Ren[3], K. X. Wei[1] and Y. D. Wang[2,**]

1. Department of Mechanical Engineering, Hunan Institute of Engineering, Xiangtan 411101, People's Republic of China

2. State Key Laboratory for Advanced Metals and Materials, University of Science and Technology Beijing, No. 30 Xueyuan Rd, Haidian District, Beijing 100083, People's Republic of China

3. X-ray Science Division, Argonne National Laboratory, Argonne, IL 60439, USA

*Corresponding author. Email: dycong@ustb.edu.cn

**Corresponding author. Email: ydwang@ustb.edu.cn

Abstract

Ni-Mn-based metamagnetic shape memory alloys have been extensively studied due to their multifunctional properties including magnetoresistance, magnetocaloric effect (MCE), and magnetic field induced stain. However, large intrinsic thermal hysteresis of these alloys sets a limit to further development for practical applications. Here, with a few atomic percent Al substitution we greatly reduced the thermal hysteresis and transformation temperature interval while maintaining the large magnetization difference (ΔM) between austenite and martensite. The effect of Al on the structural, magnetic and magnetocaloric properties of Ni-Co-Mn-Sn Heusler alloys was studied. It was disclosed that the thermal hysteresis (ΔT_{hys}) of martensitic transformation is totally dominated by the geometric compatibility condition between the two phases. Therefore, in-situ high energy X-ray diffraction technique was used to elucidate the origin of the effect of Al substitution on the magnetocaloric properties of Ni-Co-Mn-Sn multifunctional alloys. Consequently, remarkable enhancement of MCE is observed upon Al substitution and the maximum magnetic entropy change of 31.6 J/kg. K was achieved in a field of 5 T. Simultaneous achievements of the large ΔM and low ΔT_{hys} is responsible for the giant MCE in these compounds, which are quite promising for magnetocaloric applications.

Introduction

Over the last decades, many studies have been developed on Ni-Mn-based shape memory alloys due to their outstanding multifunctional properties, such as superelastic[1,2], elastocaloric effect[3,4], magnetoresistant effect[5,6], magnetocaloric effect (MCE) [7-10], magnetic field induced stain[11-13]. These properties are associated with the external-field-induced martensitic transformation (MT) in the off-stoichiometric Ni2Mn1+xX1-x (X=In, Sb or Sn) ferromagnetic shape memory alloys (FSMAs) [1,14]. Therefore, it is significant to tune the phase transition to obtain ideal MT in the practical applications of Ni-Mn-based FSMAs [15-20].

However, there are two key aspects that have to be accounted for potential applications for the MT in Ni-Mn-based alloys. On the one hand, it is necessary to obtain a high difference of magnetization between austenite and martensite (ΔM) across the first-order magnetostructural transformation. On the other hand, the large hysteresis (ΔThys) across the martensitic transition should be reduced.

Considering the value of the difference of magnetization (ΔM) between austenite and martensite is relatively small for Ni-Mn-X (X=In, Sb or Sn) ternary alloys, the Co substitution for Ni is been widely investigated which could obviously enhance the ferromagnetism in austenite and suppress the magnetic state of martensite for Ni-Co-Mn-X (X=In, Sb or Sn) alloys. It was reported that the magnetic coupling between the Mn moments on the 4a and 4b sites changed from being antiferromagnetic to ferromagnetic

by substitution of Co. As a result of the change in the magnetic structure due to the Co substitution gives rise to a significantly enhanced magnetization in the parent phase and thus a large ΔM across the transformation was obtained [21].

However, though this approach is beneficial for obtaining large ΔM, it is accompanied by pronounced hysteretic phenomena [22-24]. It is well known that the large thermal hysteresis originating from the first-order magnetostructural transformation in the Ni-Mn-based Heusler alloys always leads to a large irreversible energy loss during the successive cycling changes, which is associated with the nucleation of the new phase and the interaction of interfaces with defects [25].

An effective method employed to attempt to reduce the hysteresis of the magnetocaloric materials is through adding other alloying elements [26-30]. V. Provenzano et al. report the reduction of these hysteretic losses by alloying the compound with a small amount of iron in Gd-Si-Ge magnetocaloric materials. They found that once the hysteresis losses are considered, a greater net capacity is obtained for the iron-containing alloy [26]. It is observed that the extremely large thermal hysteresis of 75 K of the parent compound MnFe0.95P0.67Si0.33 is strongly suppressed by B substitution, resulting in a hysteresis of only 1.6 K in the MnFe0.95P0.595B0.075Si0.33 compound [27]. It should be noted that the magnetic properties (ΔM) or magnetocaloric effect (MCE) have been weakened to some extent when adding certain alloy to the parent compound. Thus, only simultaneous achieving a large ΔM and a low hysteresis can it be beneficial to obtain a novel magnetic refrigeration material.

Recently, it was found that the substitution for Sn by Al can decrease the ΔThys in Ni-Mn-Sn alloys [28]. However, the ΔM of Ni-Mn-Sn-Al alloys is extremely lower than that of Co-alloyed alloys [7]. Therefore, it is expected to simultaneously achieve high ΔM and low ΔThys through introducing Co and Al to Ni-Mn-Sn alloys, thus to tune the magnetocaloric properties.

In the present paper we will investigate in depth the combine effects of Co and Al doping on Ni-Mn-Sn alloys, focusing on the effect of Al substitution on the magnetocaloric properties of Ni-Co-Mn-Sn alloy. We hope that this study may introduce an alternative way to reduce the hysteresis between the two phases without deteriorating their magnetic properties in FSMAs.

2. Experimental

Polycrystalline ingots of Ni50-xCoxMn40Sn10-yAly (x=10, 11 and y=0, 2, 3 denote as Co10Al0, Co10Al2, Co11Al2, Co11Al3) (at. %) were prepared by repeated melting of the high-purity constituent elements in an arc furnace under argon atmosphere. Subsequently it was sealed in an evacuated quartz tube and annealed at 1273 K for 9 h followed by water quenching to ensure homogeneity. The phase transformation temperatures were measured by differential scanning calorimetry (DSC) in the temperature range of 223-473 K with cooling and heating rates of 10 K/min. The structure of the austenite and martensite phases was probed by in-situ high-energy X-ray diffraction (HEXRD) technique. The synchrotron HEXRD experiments were carried out at the 11-ID-C beamline at the Advanced Photon Source, Argonne National Laboratory. The diffraction Debye rings were collected by a two-dimensional (2D) large area detector. The magnetic properties were measured in a physical property measurement system (PPMS, Quantum Design) with a magnetic field up to 14 T.

3. Results and discussion

The DSC results of Ni40-xCo10+xMn40Sn10-yAly (x=0, 1, 3; y=0, 2, 3) alloys are shown in Fig.1. It can be seen that the large exothermic and endothermic peaks during cooling and heating corresponding to direct and reverse martensitic transformations have been detected. The characteristic transition temperatures, including the austenite start and finish (As and Af), and martensite start and finish (Ms and Mf) temperatures can be determined, as shown in Fig.1 (see Table 1 for the detailed values). With Al

substitution Sn on the basis of Ni40Co10Mn40Sn10, the transformation peaks strongly shift towards the high temperature regime. Oppositely, the replacing of Ni with Co leads transition temperatures to an obvious diminishing. It is worth noting that by introducing of minor Al the thermal hysteresis ΔThys and the transformation temperature interval ΔTint are drastically reduced. More importantly, one can also find that the Ni39Co11Mn40Sn7Al3 (Co11Al3) alloys show a very small thermal hysteresis (~8 K).

In order to study the effect of Al substitution on the magnetic properties of Ni-Co-Mn-Sn multifunctional alloys. Fig. 2 shows the temperature dependence of magnetization of Ni40Co10Mn40Sn10 (Co10Al0) and Ni39Co11Mn40Sn8Al2 (Co11Al2) alloys measured during cooling and heating cycles in a magnetic field of 4 T. It can be seen that both the thermal hysteresis and the width of the transformation are strongly suppressed by Al substitution Sn, which is agreement with the DSC results shown in Fig.1. It is clear that the high temperature austenite shows ferromagnetic feature, while the low temperature martensite is in a weak magnetic state for these two alloys. On the left of Fig. 2 are presented the M(T) curve under 4 T for Ni40Co10Mn40Sn10(Co10Al0) alloy, ΔM is determined to be 103 emu/g. Most interesting is the fact that the large magnetization difference (ΔM) between the parent phase and martensite is still persisted to 90 emu/g while the thermal hysteresis is reduced to 10 K when the replacing of Al with Sn for Ni39Co11Mn40Sn8Al2 (Co11Al2) alloy on the right of Fig. 2. Those merits are beneficial to obtain the excellent magnetocaloric effect (MCE) [9].

To evaluate the MCE of Ni40Co10Mn40Sn10 (Co10Al0) and Ni39Co11Mn40Sn8Al2 (Co11Al2) alloys, the M(H) curves at different temperatures close to austenitic transformation temperatures were measured, which are shown in Fig.3 (a) and (b) respectively. Before each measurement, the samples were first cooled to a low temperature (below Mf about 100 K) to ensure the same initial state of a fully martensite and then heated to the desired measurement temperature. This is to avoid the effect of possible residual field-induced austenite due to the incomplete transformation from austenite to martensite during decreasing field in the previous measurement. The curves were recorded during both increasing and decreasing fields, but for clarity only those recorded during increasing fields are shown in Fig. 3 (a).

The magnetic entropy change (ΔSm), one characteristic parameter for MCE, can be calculated using the Maxwell relation,

$$\Delta S_m = S_m(T,H) - S_m(T,0) = \int_0^{\mu_0 H} \frac{\partial M}{\partial T} d(\mu_0 H) \tag{1}$$

In the present study, ΔSm was estimated numerically from the isothermal M(H) curves shown in Fig. 3. The temperature dependence of ΔSm at different magnetic fields is demonstrated in Fig. 4. The maximum value of ΔSm is 14.9 J/(kg K) for Co10Al0 alloy and 31.6 J/(kg K) for Co11Al2 alloy, respectively. The ΔSm shows a tablelike peak under 5 T for both samples, which reflect the intrinsic nature of magnetocaloric effect [23]. It is evident that when the replacing of Al with Sn for Ni39Co11Mn40Sn8Al2 (Co11Al2) alloy, the magnetic entropy change ΔSm is larger than that of Ni40Co10Mn40Sn10 (Co10Al0) alloy. It is reported that the magnetic interaction is considerably complex in the off-stoichiometric Ni-Mn-based alloys especially for those with an excess of Mn, indicating that a very small change of the Mn-Mn distance due to the introducing of few Al greatly affects the magnetic properties of the sample [16].

To elucidate the origin of the effect of Al substitution on the magnetocaloric properties of Ni-Co-Mn-Sn multifunctional alloy, in-situ HEXRD experiments were performed in the temperature range of the martensitic transformation region. Fig. 5 (a) and (b) show the HEXRD patterns collected at 280 K and 260 K for Ni40Co10Mn40Sn10(Co10Al0) alloy, 370 K and 360 K for

Ni39Co11Mn40Sn8Al2(Co11Al2) alloy, respectively. It is clear that at high temperature the two samples are in the austenitic state and all the diffraction peaks can be well indexed according to the cubic austenitic structure, while at low temperature the both samples show a martensitic structure and the diffraction pattern can be well indexed according to the six-layered modulated (6M) monoclinic structure. It should be noted that there are still some diffraction peaks (such as 220 and 400 diffraction peaks) of austenite phase structure for the Ni40Co10Mn40Sn10(Co10Al0) alloy at 260 K. The corresponding lattice parameters are listed in the table 1.

It is believed that the thermal hysteresis (ΔThys) of martensitic transformation is totally dominated by the geometric compatibility condition between austenite and martensite, which is proposed by R. D. James and his coworkers [30, 31]. Based on this theory design strategy, many researchers are devoted to searching for the geometric compatibility condition [32-36], which is measured by the middle eigenvalue (λ2) of the transformation stretch matrix, represents the presence of an invariant plane between austenite and martensite. The correlation between λ2 and ΔThys was previously confirmed within the Ti-Ni-Cu stress-field-induced shape memory alloys system by J. Cui and coworkers [31]. Recently, some studies have been also conducted to develop this geometric nonlinear theory in Ni-Mn based magnetic-field-driven shape memory alloys [35-38]. It comes to the conclusion from the published date that, the closer to one the middle eigenvalue (λ2) is, the more geometric compatible the austenite and the martensite are, and thus the lower the thermal hysteresis is [30]. By using algorithms for the cubic to monoclinic transformation from the corresponding measured lattice parameters (listed in table 1) for our samples, the middle eigenvalue (λ2) are calculated to be 0.9952 for Ni40Co10Mn40Sn10(Co10Al0) alloy, and 0.9961 for Ni39Co11Mn40Sn8Al2(Co11Al2) alloy, respectively. This indicates that our Ni39Co11Mn40Sn8Al2(Co11Al2) sample with small thermal hysteresis closely satisfies the geometric compatibility condition. Therefore, we can apply this theory to control and optimize the thermal hysteresis by fine-tuning the lattice parameters between the austenite and the martensite.

4. Conclusions

In conclusion, the effects of doping Al atoms for Sn on the martensitic transformation and magnetocaloric effect in Ni-Co-Mn-Sn Heusler alloys have been investigated. The thermal hysteresis and transformation temperature interval have been greatly reduced, while the large magnetization difference (ΔM) between austenite and martensite has been maintained by Al substitution for Sn. Consequently, remarkable enhancement of MCE is observed upon Al substitution and the large magnetic entropy change have been achieved in a field of 5 T. Meanwhile, we have found our Ni39Co11Mn40Sn8Al2 alloy that closely satisfies the geometric compatibility condition by in-situ high energy X-ray diffraction technique. Therefore, this alloy shows potential for magnetocaloric applications.

Acknowledgments

We acknowledge the support from the National Natural Science Foundation of China (Nos. 51701070 and 51527801), the Provincial Natural Science Foundation of Hunan (Grant No.2019JJ50101), the Scientific Research Fund of Hunan Province Education Department (Grant No.17A046), and the State Key Laboratory for Advanced Metals and Materials (Grant No. 2016-T01). Use of the Advanced Photon Source was supported by the U.S. Department of Energy, Office of Science, Office of Basic Energy Science, under Contract No. DE-AC02-06CH11357.

Reference

[1] R. Kainuma, Y. Imano, W. Ito, Y. Sutou, H. Morito, S. Okamoto, O. Kitakami, K. Oikawa, A. Fujita, T. Kanomata, and K. Ishida, Nature (London) **439**, 957 (2006).

[2] H. E. Karaca, I. Karaman, B. Basaran, Y. Ren, Y. I. Chumlyakov, and H. J. Maier, Adv. Funct. Mater. **19**, 983 (2009).

[3] Z. Yang, D.Y. Cong, X.M. Sun, Z.H. Nie, and Y.D. Wang, Acta Mater. **127**, 33 (2017).

[4] F. Xiao, M. J. Jin, J. Liu, and X.J. Jin, Acta Mater. **96**, 292 (2015).

[5] V. K. Sharma, M. K. Chattopadhyay, K. H. B. Shaeb, Anil Chouhan, and S. B. Roy, Appl. Phys. Lett. **89**, 222509 (2006).

[6] K. Koyama, H. Okada, K. Watanabe, T. Kanomata, R. Kainuma, W. Ito, K. Oikawa, and K. Ishida, Appl. Phys. Lett. **89**, 182510 (2006).

[7] R. Kainuma, Y. Imano, W. Ito, Y. Sutou, H. Morito, S. Okamoto, O. Kitakami, K. Oikawa, A. Fujita, T. Kanomata, and K. Ishida, Nature (London) **439**, 957 (2006).

[8] T. Krenke, E. Duman, M. Acet, E. F. Wassermann, X. Moya, L. Mañosa, and A. Planes, Nat. Mater. **4**, 450 (2005).

[9] T. Gottschall, K. P. Skokov, R. Burriel, and O. Gutfleisch, Acta Mater.**107**,1 (2016).

[10] X. Moya, S. Kar-Narayan, and N. D. Mathur, Nat Mater.**13**,439 (2014).

[11] K. Ullakko, J. K. Huang, C. Kantner, R. C. O'Handley, and V. V. Kokorin, Appl. Phys.Lett. **69**, 1966 (1996).

[12] A. Sozinov, A. A. Likhachev, N. Lanska, and K. Ullakko, Appl. Phys. Lett. **80**, 1746 (2002).

[13] M. Chmielus, X. X. Zhang, C. Witherspoon, D. C. Dunand, and P. Müllner, Nat Mater.**8**,863 (2009).

[14] B. Zhang, X. X. Zhang, S.Y. Yu, J. L. Chen, Z. X. Cao, and G. H. Wu, Appl. Phys. Lett. **91**, 012510 (2007).

[15] B. M. Wang, Y. Liu, P. Ren, B. Xia, K.B. Ruan, J. B. Yi, J. Ding, X. G. Li, and L. Wang, Phys. Rev. Lett. **106**, 077203 (2011).

[16] Y. Sutou, Y. Imano, N. Koeda, T. Omori, R. Kainuma, K. Ishida, and K. Oikawa, Appl. Phys. Lett. **85**, 4358 (2004).

[17] J. H. Chen, N. M. Bruno, I. Karaman, Y. J. Huang, J. G. Li, and J. H. Ross Jr, Acta

Mater.**105**,176 (2016).

[18] J. A. Monroe, I. Karaman, B. Basaran, W. Ito, R. Y. Umetsu, R. Kainuma, K. Koyama, and Y. I. Chumlyakov, Acta Mater. **60**, 6883 (2012).

[19] T. Krenke, E. Duman, M. Acet, and E. F. Wassermann, Phys Rev B. **75**,104414 (2017).

[20] A. Smith, C. R. H. Bahl, R. Bjørk, K. Engelbrecht, K. K. Nielsen, and N. Pryds, Adv Energy Mater. **2**,1288 (2012).

[21] S. Y. Yu, L. Ma, G. D. Liu, Z. H. Liu, J. L. Chen, Z. X. Cao, G. H. Wu, B. Zhang and X. X. Zhang, Appl. Phys. Lett. 90, 24250 (2007).

[22] D.Y. Cong, S. Roth, and L. Schultz, Acta Mater. **60**, 5335 (2012).

[23] L. Huang, Y. H. Qu, D. Y. Cong, X. M. Sun, and Y. D. Wang, Shap. Mem. Superelasticity **3**, 218 (2017).

[24] Z. B. Li, Y. W. Jiang, Z. Z. Li, C. F. Sanchez Valdes, J. L. Sanchez Llamazares, B. Yang, Y. D. Zhang, C. Esling, X. Zhao, and L. Zuo, IUCrJ **5**, 54 (2018).

[25] F. X. Hu, J. Wang, J. Shen, B. Gao, J. R. Sun, and B. G. Shen, J. Appl. Phys. **105**, 07A940 (2009).

[26] V. Provenzano, A. J. Shapiro, and R. D. Shull, Nature (London) **429**, 853 (2004).

[27] F. Guillou, G. Porcari, H. Yibole, N. van Dijk, and E. Brück, Adv. Mater. **26**, 2671 (2014).

[28] R. L. Wang, J. B. Yan, L.S. Xu, V.V. Marchenkov, S. S. Chen, S.L. Tang, and C.P. Yang, Solid State Communications **151**, 1196 (2011).

[29] Z. B. Li, S. Y. Dong, Z. Z. Li, B. Yang, F. Liu, C. F. Sánchez-Valdés, J. L. Sánchez Llamazares, Y. D. Zhang, C. Esling, X. Zhao, and L. Zuo, Scr. Mater.**159**,113 (2019).

[30] J. Cui, Y. S. Chu, O. O. Famodu, Y. Furuya, J. Hattrick-Simpers, R. D. James, A. Ludwig, S. Thienhaus, M. Wuttig, Z. Zhang, and I. Takeuchi, Nat. Mater. **5**, 286 (2006).

[31] Y. Song, X. Chen, V. Dabade, T. W. shield, R. D. James, Nature **502**,85 (2013).

[32] J. Liu, Y. Gong, Y. You, X. You, B. Huang, X. Miao, G. Xu, F. Xu, and E. Brück, Acta Mater. (2019), in press. https://doi.org/10.1016/j.actamat.2019.05.066.

[33] Z. Zhang, R.D. James, and S. Müller, Acta Mater. **57**,4332 (2009).

[34] C. Chluba, W. Ge, R. L de Miranda, J. Strobel, L. Kienle, E. Quandt, and M. Wuttig,

Science **348**, 1004 (2015).

[35] V. Srivastava, X. Chen, and R. D. James, Appl. Phys. Lett. **97**, 014101 (2010).

[36] D. W. Zhao, J. Liu, X. Chen, W. Sun, Y. Li, and M.X. Zhang, Acta Mater. **133**, 217 (2017).

[37] J. Liu, T. Gottschall, K. P. Skokov, J. D. Moore, and O. Gutfleisch, Nat. Mater. **11**, 620 (2012).

[38] D. Y. Cong, L. Huang, V. Hardy, D. Bourgault, X. M. Sun, Z. H. Nie, M. G. Wang, Y. Ren, P. Entel, and Y. D. Wang, Acta Mater. **146**,142 (2018).

Figure Captions

FIG.1. DSC curves of the $Ni_{40-x}Co_{10+x}Mn_{40}Sn_{10-y}Al_y$ (x=0, 1, 3; y=0, 2, 3) alloys.

FIG.2. Isofield magnetization curves recorded at H = 4 T upon cooling and heating for $Ni_{40}Co_{10}Mn_{40}Sn_{10}(Co_{10}Al_0)$ and $Ni_{39}Co_{11}Mn_{40}Sn_8Al_2(Co_{11}Al_2)$ alloys.

FIG.3. M(H) curves measured at different temperatures close to the austenitic transformation temperatures. For clarity, only the curves during increasing magnetic fields are displayed. a) for $Ni_{40}Co_{10}Mn_{40}Sn_{10}$ $(Co_{10}Al_0)$ and b) $Ni_{39}Co_{11}Mn_{40}Sn_8Al_2$ $(Co_{11}Al_2)$ alloys.

FIG. 4. Magnetic entropy change ΔS_m as functions of temperature and magnetic field for for $Ni_{40}Co_{10}Mn_{40}Sn_{10}(Co_{10}Al_0)$ and $Ni_{39}Co_{11}Mn_{40}Sn_8Al_2(Co_{11}Al_2)$ alloys.

FIG. 5. (a, b) High-energy X-ray diffraction patterns experimentally collected at 280 K and 260 K for (a) at 280 K and 260 K for $Ni_{40}Co_{10}Mn_{40}Sn_{10}(Co_{10}Al_0)$ alloy, 370 K and 360 K for $Ni_{39}Co_{11}Mn_{40}Sn_8Al_2(Co_{11}Al_2)$ alloy (b), respectively.

Table 1 Martensitic and austenitic transformation characteristic temperatures (K), transformation thermal hysteresis ΔT_{hys} (K), phase transformation interval ΔT_{int} (K) for the $Ni_{40-x}Co_{10+x}Mn_{40}Sn_{10-y}Al_y$ (x=0, 1, 3; y=0, 2, 3) alloys. The letters "M" and "A" denote martnensitic and austentic transformations, respectively.

Table 2 The lattice parameters of austenitic and martensitic phase listed at 280 K and 260 K for $Ni_{40}Co_{10}Mn_{40}Sn_{10}(Co_{10}Al_0)$ alloy, 370 K and 360 K for $Ni_{39}Co_{11}Mn_{40}Sn_8Al_2(Co_{11}Al_2)$ alloy, respectively. The letters "A" and "6M" in the indices denote austenite and six-layered modulated martensite, respectively. The coordinates of
the figures are expressed with respect to the scattering vector Q with its length $Q = 2\pi/d = 4\pi \sin\theta/\lambda$, with d being the interplanar spacing and 2θ the diffraction angle.

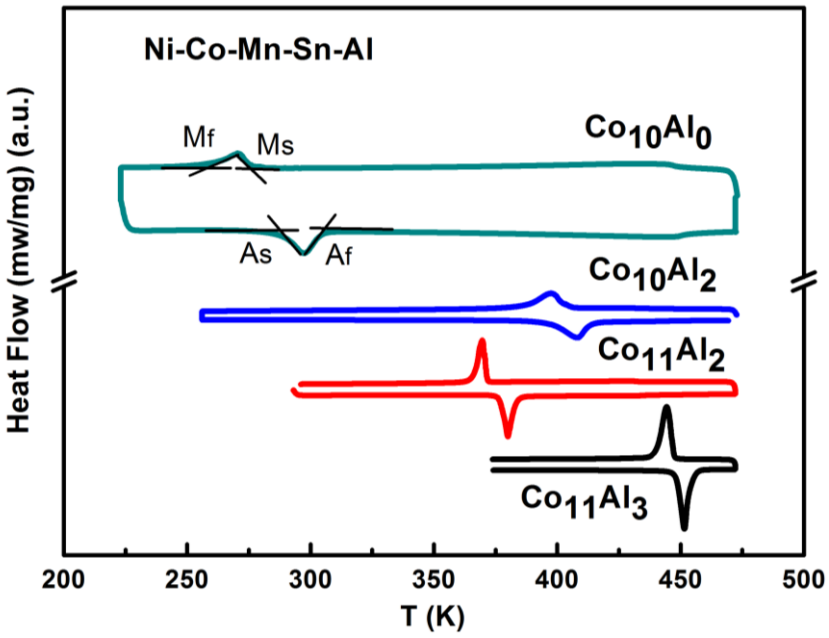

FIG.1

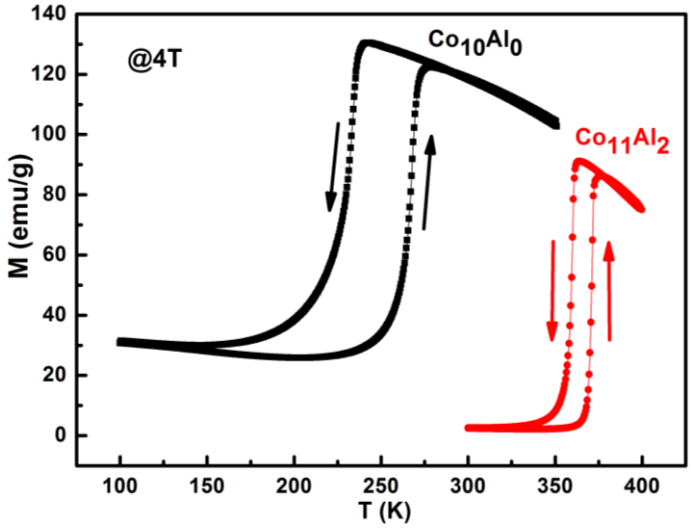

FIG. 2

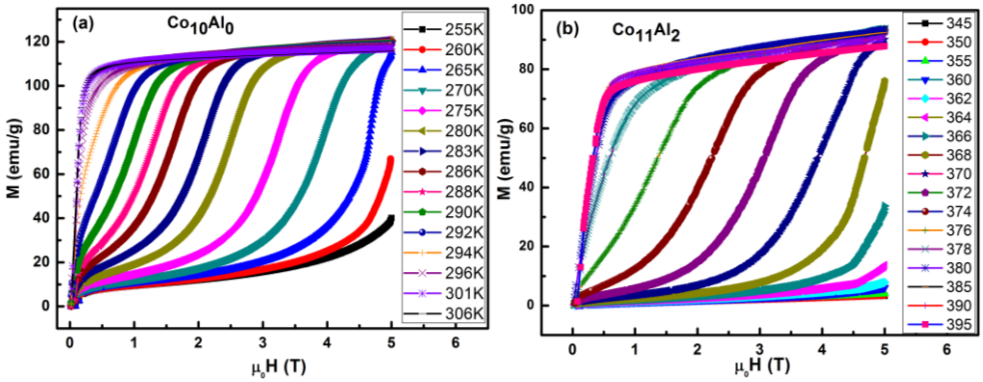

FIG.3

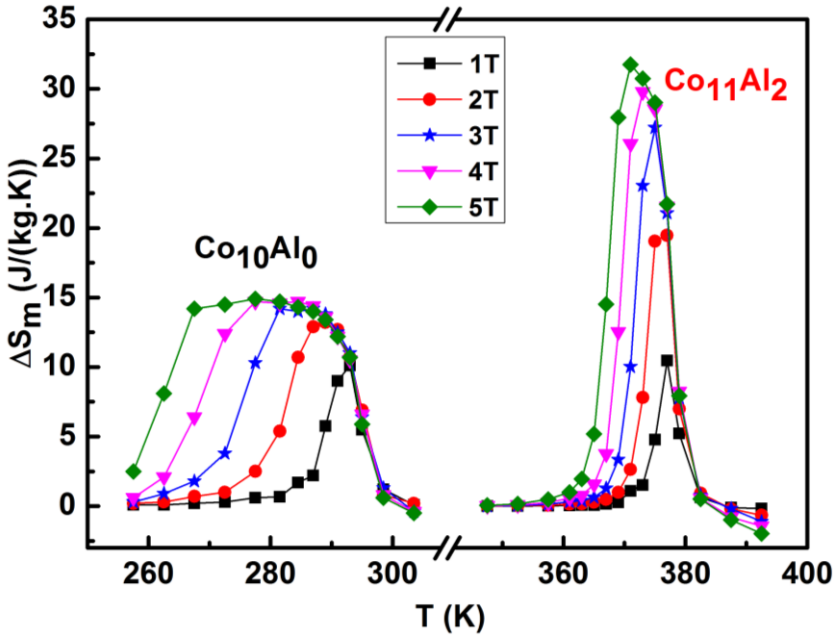
1T
2T
3T
4T
5T
Co10Al0
Co11Al2
ΔSm (J/(kg.K))
T (K)

FIG. 4

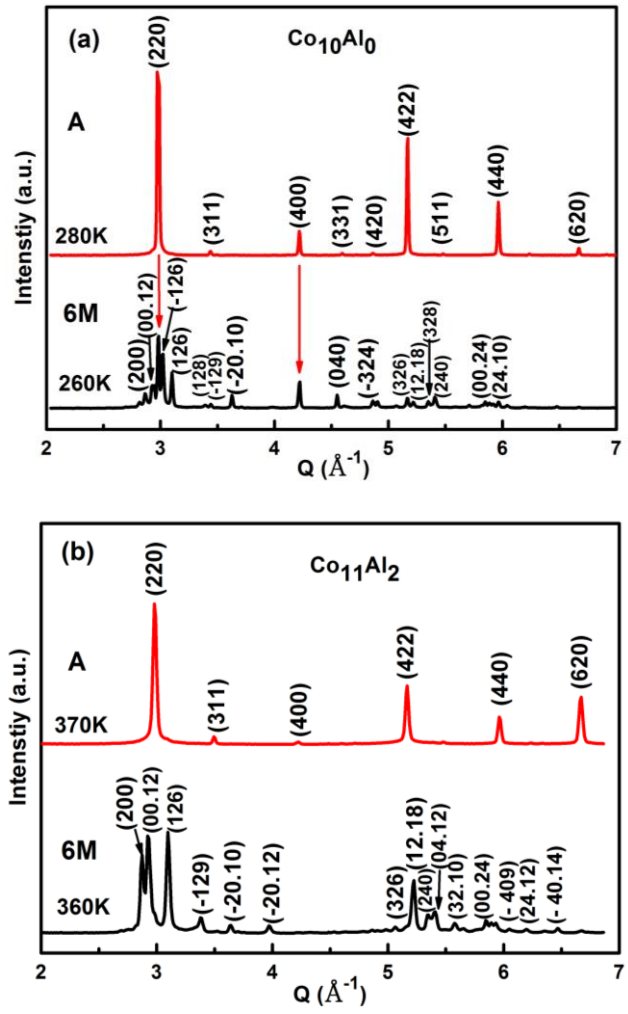
(a)
Co10Al0
A
280K
6M
260K
Intenstiy (a.u.)
Q (Å-1)
(b)
Co11Al2
A
370K
6M
360K
Intenstiy (a.u.)
Q (Å-1)

FIG. 5

Table 1

Alloy	M_s(K)	M_f(K)	A_s(K)	A_f(K)	ΔT_{hys} (K)	ΔT_{int}(K)
$Co_{10}Al_0$	275	260	288	306	31	15
$Co_{10}Al_2$	405	388	398	415	10	17
$Co_{11}Al_2$	372	366	376	382	10	6
$Co_{11}Al_3$	447	440	449	455	8	7

Table 2

Alloy	a_A(Å)	a_M(Å)	b_M(Å)	c_M(Å)	β(°)	λ_2
$Co_{10}Al_0$	5.960	4.395	5.524	25.743	93.60	0.9952
$Co_{11}Al_2$	5.957	4.391	5.559	25.842	93.82	0.9961